ACS APPLIED MATERIALS & INTERFACES

Research Article

www.acsami.org

Scab-Inspired Cytophilic Membrane of Anisotropic Nanofibers for Rapid Wound Healing

Yanli Xi,[†,‡] Hua Dong,[†] Kang Sun,[†] Hongliang Liu,[†] Ruiming Liu,[†,§] Yuansen Qin,[†,§] Zuojun Hu,[†,§] Yong Zhao,[†] Fuqiang Nie,[†] and Shutao Wang*[,†]

[†]Beijing National Laboratory for Molecular Sciences (BNLMS), Key Laboratory of Organic Solids, Institute of Chemistry, Chinese Academy of Sciences, Beijing 100190, People's Republic of China

[‡]School of Public Health, Jinlin University, Changchun 130021, People's Republic of China

[§]Department of Vascular Surgery, The First Affiliated Hospital of Sun Yat-Sen University, Guangzhou 510080, People's Republic of China

S *Supporting Information*

ABSTRACT: This work investigates the influence of cytophilic and anisotropic nanomaterials on accelerated cell attachment and directional migration toward rapid wound healing. Inspired by the anisotropic protein nanofibers in scab, a polyurethane (PU) nanofibrous membrane with an aligned structure was fabricated. The membrane showed good affinity for wound-healing-related cells and could guide cell migration in the direction of PU nanofibers. Also, the morphology and distribution of F-actin and paxillin of attached cells were influenced by the underlying nanofibers. The randomly distributed PU nanofibers and planar PU membrane did not show a distinct impact on cell migration. This scab-inspired cytophilic membrane is promising in applications as functional interfacial biomaterials for rapid wound healing, bone repair, and construction of neural networks.

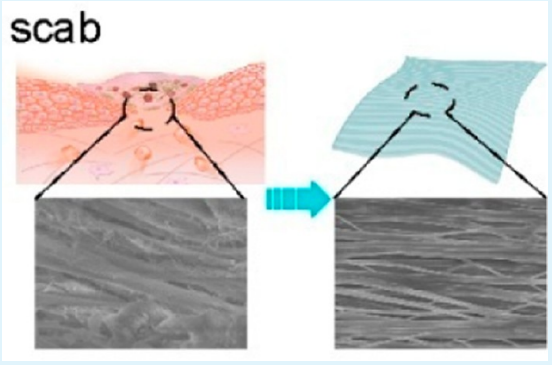

KEYWORDS: *cytophilic, anisotropic nanofibrous membranes, wound healing, cell attachment, cell migration*

INTRODUCTION

Scab, a hard and reddish glob, is essential in the natural process of wound healing, although patients do not like its appearance. As a natural dressing material, scab plays multifunctional roles in promoting wound healing, such as blocking blood leakage, protecting underlying tissue from pathogen invasion, and recruiting cells for repairing the injured skin.[1−3] For artificial dressing materials that are often employed as skin substitutes to aid skin regeneration,[4] various materials have been applied in forms of hydrocolloid dressings,[5] hydrogel,[6−8] and nanofibers.[9−11] Most of these materials are generally fabricated with emphasis on the antipathogen property or biocompatibility. However, accelerating wound healing still goes beyond the function of these current dressing materials. Accelerating wound healing or rapid wound healing can efficiently reduce the risk of infection and minimize the wound area. Therefore, developing dressing materials toward rapid wound healing becomes a great challenge.

Herein, by investigating the surface structure of scab, we fabricated a cytophilic anisotropic nanofibrous membrane that could be used for rapid wound healing. Undoubtedly, scab is an optimized dressing material designed by nature for wound healing. While many studies have focused on the growth factors and cytokines in scabs,[12] the nanoscale fibrous structure in scab is generally neglected and the microscale of fibers is often applied in commercial products (Figure S1, Supporting Information). We found that there were locally anisotropic nanofibers on the inner surface of scab (Scheme 1). Inspired by this, we designed and fabricated a nanofibrous membrane by electrospinning polyurethane (PU) into anisotropic nanofibers. The PU nanofibers showed excellent cytophilicity for different types of cells that were involved in the process of wound healing. Furthermore, we showed that this anisotropic nanofibrous membrane can guide the directional cell migration. This scab-inspired cytophilic and direction-guiding nanofibrous membrane can be used as a new type of dressing material for rapid wound healing.

EXPERIMENTAL METHODS

Electrospinning. The electrospinning process was carried out in a typical electrospinning set. The electrode distance was between 15 and 20 cm, the direct-current voltage was 8−11 kV, the distance between the two grounded parallel metal electrodes was 2 cm, and the concentration of PU was 8% (m/m) in mixed solution of tetrahydrofuran/*N*,*N*-dimethylformamide (8/2, m/m).

Received: February 4, 2013
Accepted: April 29, 2013
Published: April 29, 2013

   dx.doi.org/10.1021/am4004683 | *ACS Appl. Mater. Interfaces* 2013, 5, 4821−4826

Scheme 1. Schematic Illustration of a Scab-Inspired Anisotropic Nanofibrous Membrane[a]

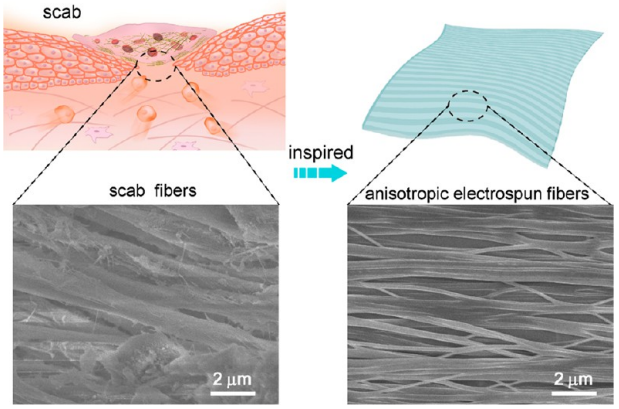

[a]The inner side of scab contains anisotropic protein nanofibers, which is important in recruiting cells for repairing wound regions. The inner structure of the scab inspired the design of an anisotropic nanofibrous membrane for rapid wound healing.

Nanofibers Characterization. Scanning electron microscopy (SEM) images were obtained on a field-emission scanning electron microscope (JEOL JSM-6700F, Japan).

Cell Culture. Human umbilical vein endothelial cells (HUVECs; ATCC, Manassas, VA) were cultured in Dulbecco's modified Eagle's medium (DMEM; with 1 g·L of glucose) supplemented with 2% (v/v) fetal bovine serum (FBS; Gibco-Invitrogen, Carlsbad, CA), penicillin/streptomycin (P/S; 100 μg/mL, Sigma-Aldrich), at 37 °C in a humidified atmosphere with 5% (v/v) CO_2 in a 6 cm^2 culture dish (Nunc, Roskilde, Denmark). Mouse embryonic fibroblasts (NIH 3T3, ATCC) were maintained in DMEM mixed with 10% (v/v) FBS and P/S (100 μg/mL). Human lens epithelial cells (SRA 01-04, ATCC) were routinely cultivated in Minimum Essential Media (MEM; Gibco-Invitrogen) supplemented with 10% (v/v) FBS. Cells were dissociated from culture dishes by trypsin/ethylenediaminetetraacetic acid [EDTA; 0.25% trypsin and 0.02% EDTA in phosphate-buffered saline (PBS), Gibco-Invitrogen]. Then, the membranes (1 cm × 1 cm) were put in six well plates and sterilized by UV light before cell seeding.

Cell Viability Assay. The cell viability was measured by the (methylthiazolyldiphenyl)tetrazolium bromide (MTT) assay. In brief, the membranes were cultured with HUVECs at a density of 1×10^5 cells/mL in six well plates and incubated for 24 h. Glasses were chosen as the control. After incubation period, the medium was removed and a fresh medium containing a 5 mg/mL MTT solution was added to each well and incubated for an additional 4 h at 37 °C. Finally, the medium containing MTT was removed, and cells were lysed with dimethyl sulfoxide. The absorbance at 490 nm was measured using a microplate reader (Tecan infinite M200 TECAN).

Cell Attachment Assay. Three pieces of membranes were cultured with HUVECs at a density of 1×10^6 cells/mL in six well plates and incubated for 15, 30, and 45 min. The samples were washed three times with PBS and fixed with 4% paraformaldehyde for 30 min, followed by gentle washing with PBS three times. Then the samples were immersed in 0.2 mg/mL 4′,6-diamidino-2-phenylindole (DAPI) for 5 min and washed three times with PBS. Each sample was captured using a fluorescence microscope (Olympus XSP-63XD, Japan) and analyzed using *Image-Pro Plus 6.0* software.

Wound Closure Assay. The stopper assay method was adopted to construct a wound healing model. A glass capillary (0.5 mm diameter) was put in the middle of the membrane. Then cells were seeded on the surfaces and cultured for 24 h, and the glass capillary was removed and washed several times with PBS to remove cell debris. A gap of cells was formed on the membrane, and then the membranes were set in a humidified atmosphere for cell migration experiments. The average migration areas from their original positions were recorded by a phase contrast microscope equipped with a digital camera (Olympus, Japan) and analyzed using *Image-Pro Plus 6.0* software at 2, 6, and 10 h, respectively. All assays were performed at least three times in triplicate.

Statistical Analysis. All data were expressed as mean ± standard deviation (SD). Statistical analyses were performed by one-way analysis of variance (ANOVA) using *SPSS* (version 17.0) software. Each experiment was repeated three times. In a comparison between two groups of data, a value of $P < 0.05$ was considered significant.

Environmental Scanning Electron Microscopy (ESEM). An environment scanning electron microscope (FEI Quanta 200) was used to image the cells on the different membranes. To prepare samples for ESEM observation, cells were washed with PBS and fixed with 2.5% glutaraldehyde overnight. After fixing, cells were rinsed in PBS twice and dehydrated by sequential incubations in 30%, 50%, 70%, 80%, 95%, and pure ethanol for 10 min at room temperature. The samples were dried with critical CO_2 drying for subsequent ESEM observation.

Confocal Microscopy. The HUVECs were fixed with 4% paraformaldehyde for 30 min, followed by washing with PBS three times. The cells were treated with 0.1% Triton X-100 for 10 min, washed twice with PBS, and permeabilized with a rhodamine-labeled phalloidin solution for 45 min at room temperature and with 0.2 mg/mL DAPI for 5 min. The cells were finally washed three times with PBS and then immersed in PBS. Each sample was captured using a confocal microscope (Olympus XSP-63XD, Japan).

RESULTS AND DISCUSSION

We first studied the structures of scab that was formed at the third day after rat skin was injured. From Scheme 1, fibrin fibers in the scab exhibited anisotropic structures with diameters of hundreds of nanometers. Anisotropic nanofibrous structures exist widely in nature, including self-assembled collagen nanofibers and nanofibrillated cellulose.[13,14] In scab, the anisotropic nanofibrous structures contribute to the function of recruiting cells, which is important for reepithelialization.[1] Thus, we prepared artificial anisotropic PU nanofibers by electrospinning. Electrospinning is a facile method for fabricating polymer nanofibers with controllable orientation.[15] Also, PU is a widely studied polymer that exhibits good biocompatibility and can be electrospun into nanofibers easily.[16] For comparison, we also prepared random nanofibrous and planar membranes by electrospinning and spin coating, respectively. Figure 1a shows the SEM images of the three as-prepared membranes. The diameters of the nanofibers were in the range of 200−500 nm. In the anisotropic nanofibrous membranes, most of the fibers were arranged in parallel to each other, while in the random nanofibrous membranes, fibers distributed randomly. For the planar membrane, the surface did not contain obvious nanostructures compared to nanofibrous membranes.

To examine the cell affinity of an anisotropic nanofibrous membrane, we performed cell attachment experiments. We chose HUVECs because they are endothelial cells that contribute to angiogenesis in wound healing. We first examined possible cytotoxicity of nanofibers.[17] All of the membranes in the experiments exhibited no harm to cells, as the cell viability was unchanged after 24 h of incubation (Figure S2, Supporting Information). We incubated cells on each substrate for 15, 30, and 45 min, respectively. The volume of cell suspension was 2 mL, and the cell density was 1×10^6 cells/mL. We counted the number of cells attached on the three types of membranes. Figure 1a shows the fluorescence microscopic images of the cells attached on the membranes after 15 min. The number of cells attached on the anisotropic nanofibrous, random nanofibrous, and planar membranes were 5236 ± 2313, 2252 ± 683,

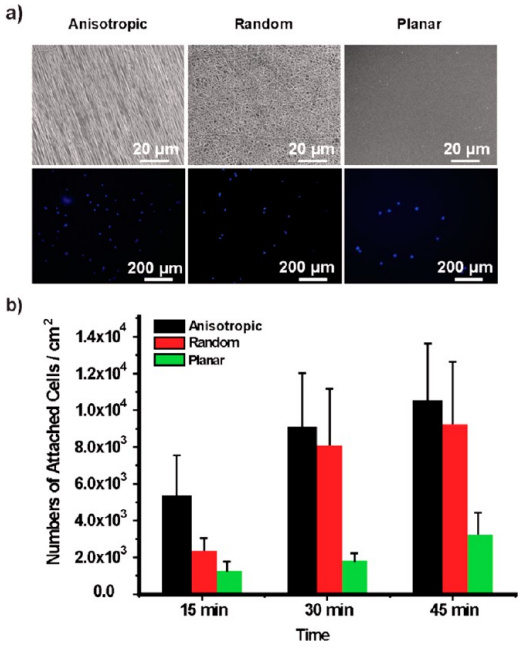

Figure 1. (a) Top: SEM images of the anisotropic nanofibrous membrane, random nanofibrous membrane, and planar membrane. Anisotropic and random membranes were fabricated by electrospinning, and the planar membrane was fabricated by spin coating. Bottom: Fluorescence microscopic images showing that there are more cells attached on the anisotropic nanofibrous membranes than on the others in first 15 min. (b) Number of cells attached on the membranes increases time dependently. Three independent experiments were carried out. Data were expressed as a percentage of the control value (mean ± SD).

and 1143 ± 521, respectively. It is worth noting that cells attached on the anisotropic nanofibrous membranes were 2 times as many as those on the random nanofibrous membranes and 4 times as many as those on the planar menbranes. Figure 1b shows that the number of attached cells increased with an increase of the incubation time for all membranes. The number of cells attached on the anisotropic nanofibrous membrane were larger compared to the other two, especially after incubation for 15 min ($P < 0.05$). The distinct cytophilicity of the anisotropic nanofibrous membrane could be attributed to the anisotropic structure. First, compared to the planar membrane, the nanofibrous membrane provides more sites for interaction with cells in the nanoscale. Second, the scab-inspired anisotropic structure is probably more advantageous than the random structure for cell attachment. Previous reports have indicated that the anisotropic structure was favorable to cell growth.[18,19] However, longer times (i.e., 30 and 45 min) of incubation led to reduced differences in the cell numbers between the anisotropic and random nanofibrous membrane, while for the planar membrane, the number of attached cells was almost one-third of the other two ($P < 0.05$). When cells were allowed to interact with the membranes for 24 h, the nanostructures did not show distinct differences in promoting cell attachment any longer. Therefore, for application in rapid cell attachment, the anisotropic structure is more advantageous than random and planar structures.

We examined the influence of the anisotropic structure of the nanofibrous membrane on cell migration. We tested four types of membranes: anisotropic-latitude nanofibrous membranes in which the orientation of the fibers was perpendicular to the wound edges, anisotropic-longitude nanofibrous membranes in which the orientation of the fibers was parallel to the wound edges, random nanofibrous membranes, and planar membranes. For cells, besides HUVECs, we also tested fibroblast cells (mouse embryonic fibroblast cells, NIH 3T3 cells) and epithelial cells (human lens epithelial cells, SRA01-04 cells), which are involved in the proliferation stage of wound healing.[1,20] To quantitatively compare the differences in cell migration between the four membranes, we constructed a wound healing assay model by an improved stopper assay method.[21−23] In brief, we used a glass capillary to lay on the surfaces of the nanofibers and seeded cells. When the cell reached confluence, we removed the glass capillary. After 10 h of incubation, we defined wound edges by a gap of cells. Using this model, we first observed the wound healing process by monitoring the migration of HUVECs into wound regions under a microscope, as shown in Figure 2. Figure 2a shows cell migration at different times (i.e., 0, 2, 6, and 10 h) after the wound model was established. As time increased, more and more cells migrated into the wound regions on the anisotropic-latitude, random, and planar membranes. For the anisotropic-longitude membrane, however, few cells migrated into the wound regions within 10 h. To quantatively compared the

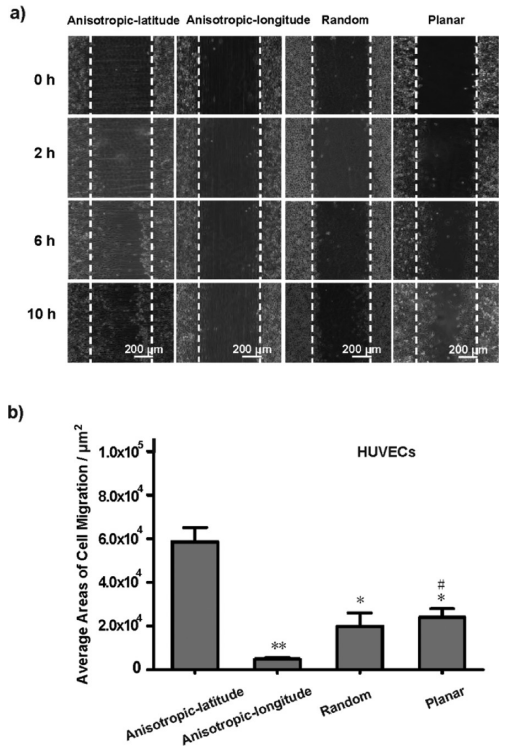

Figure 2. Anisotropic nanofibrous membranes directing migration of HUVECs. (a) Among the four types of membranes, the fastest cell migration was observed on membranes with nanofibers anisotropic toward the wound region. Cells on the random nanofibrous and planar membranes showed a medium rate of migration. The slowed migration was found on the membrane with nanofibers anisotropic along the wound region. (b) Average areas of cells that migrated into the wound region 10 h after the wound model was established. The areas were calculated by subtracting the cell area at 0 h from that at 10 h. Three independent experiments were carried out. Data were expressed as a percentage of the control value (mean ± SD): (**) $P < 0.01$ vs anisotropic-latitude membrane; (*) $P < 0.05$ vs anisotropic-latitude membrane; (#) $P < 0.05$ vs anisotropic-longitude membrane.

dx.doi.org/10.1021/am4004683 | ACS Appl. Mater. Interfaces 2013, 5, 4821−4826

differences in cell migration between the four membranes, we repeated the experiments three times and calculated the average areas of cell migration by subtracting the cell area at 0 h from that at 10 h (Figure 2b). Among the four membranes, cell migration areas were largest on the anisotropic-latitude nanofibrous membranes, which was 3 times that on the random nanofibrous and planar membranes ($P < 0.05$). For the anisotropic-longitude nanofibrous membranes, few cells appeared in the wound area. The migration areas on the anisotropic-longitude nanofibrous membranes were even smaller than those on the random nanofibrous and planar membranes. Although the anisotropic-latitude and anisotropic-longitude nanofibrous membranes had similar morphologies, the orientation showed a direct influence on cell migration. As for the random nanofibrous and flat planar membranes, the difference between the planar and anisotropic-longitude nanofibrous membranes was more distinguishable ($P < 0.05$) than that between the random and anisotropic-longitude nanofibrous membranes. For NIH 3T3 and SRA 01-04 cells, the migration areas on the anisotropic-latitude nanofibrous membranes were both larger than those on the other membranes ($P < 0.01$ for NIH 3T3 and $P < 0.05$ for SRA 01-04; Figures 3 and 4). For NIH 3T3 cells, the area on the anisotropic-latitude nanofibrous membrane was about 33.8-fold larger than that on the anisotropic-longitude nanofibrous membrane, compared to 18.7-fold for SRA 01-04 and 12.2-fold for HUVECs. This result shows that the migration of fibroblast cells is more sensitive to the underlying topography, compared to epithelial and endothelial cells in our experiments. For all three types of cells in the experiment, we can see that only when nanofibers were anisotropic and perpendicular to the long axis of the wound was cell migration obviously promoted.

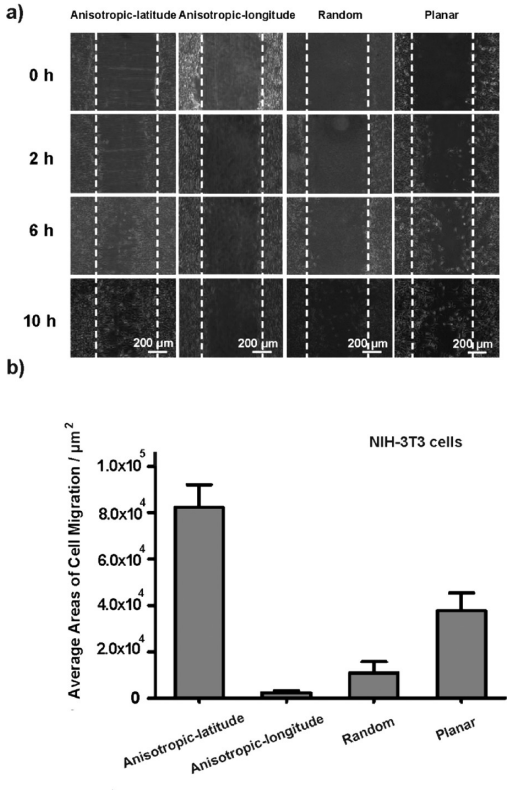

Figure 3. (a) Migration of NIH 3T3 cells on the anisotropic-latitude, anisotropic-longitude, random, and planar membranes at 0, 2, 6, and 10 h after the wound was formed. Cells on the anisotropic-latitude membranes show more promoted migration than other membranes. (b) Average areas of cells migrating into the wound areas at 10 h on various membranes. The cell density was 2×10^6 cells/mL. Three independent experiments were carried out. Data were expressed as a percentage of the control value (mean ± SD).

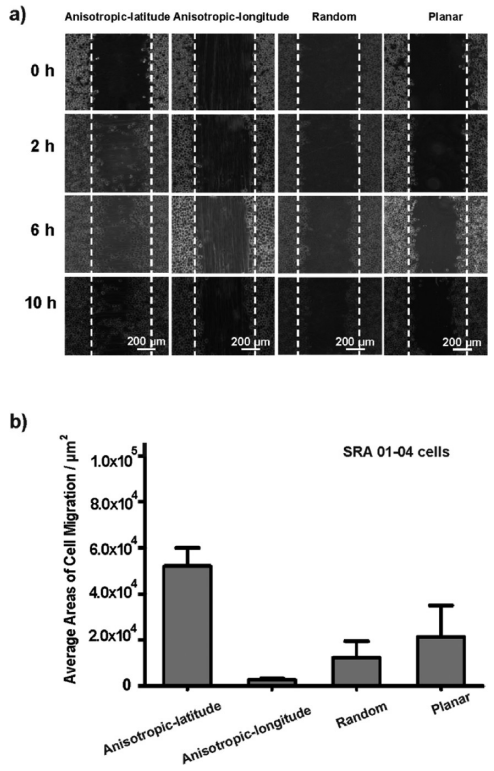

Figure 4. (a) Migration of SRA 01-04 cells on the anisotropic-latitude, anisotropic-longitude, random, and planar membranes at 0, 2, 6, and 10 h after the wound was formed. (b) Average areas of cells migrating into the wound areas at 10 h on various membranes. The cell density was 3×10^6 cells/mL. Three independent experiments were carried out. Data were expressed as a percentage of the control value (mean ± SD).

Besides cell area, cell migration can also be characterized by cell morphology and the expression of F-actin and paxillin.[24,25] To examine the relationship between the alignment of nanofibers and morphology of the cells, we observed HUVECs on anisotropic, random nanofibrous, and planar membranes on ESEM. In Figure 5a, the cells on membranes of anisotropic nanofibers presented a fiber-dependent bipolar morphology. The length axes of the cells were along the direction of the nanofibers. The bipolar morphology implies that the anisotropic orientation provided a favorable microenvironment for cell migration. While on the random nanofibrous membranes, the cells exhibited polygonal morphology (Figure 5b), cells also exhibited polygonal shapes on the planar membranes (Figure 5c). For polygonal cells, the direction of migration is random. Similar results were found for NIH 3T3 and SRA01-04 cells (Figure 6). Only nanofiber-induced bipolar morphology was found on anisotropic membranes. To examine the impact of the alignment of the nanofibers on the distribution of cytoskeleton proteins, we stained F-actin of attached cells and obeserved them under a fluorescent microscope. We found that F-actin distributed along the orientation of the nanofibers (Figure 5d) on the anisotropic nanofibrous membrane, while for the two other membranes, it

dx.doi.org/10.1021/am4004683 | ACS Appl. Mater. Interfaces 2013, 5, 4821−4826

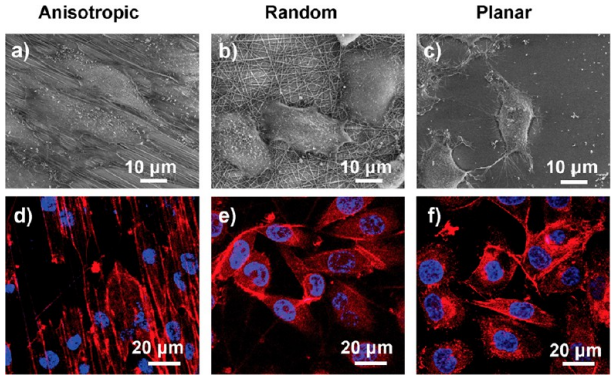

Figure 5. (a–c) ESEM images showing different morphologies of HUVECs on the anisotropic nanofibrous, random nanofibrous, and planar membranes after incubation in DMEM containing 2% FBS for 24 h. Cells on the anisotropic nanofibrous membrane presented a bipolar shape, while exhibiting round or irregular shape on the random or planar membrane. (d–f) Confocal micrographs illustrating F-actin (red) and nuclei (blue) of fluorescent-stained HUVECs seeded on different membranes after incubation of the cells for 10 h. F-actin exhibited uniform direction and elongated along the anisotropic nanofibers (d) and did not show a directional distribution on the random or planar membranes (e and f).

was normally distributed. Because cell migration involves the dynamic behaviors of the actin cytoskeleton, which involved polymerization and depolymerization of actin filaments,[26,27] by investigation of the distribution of F-actins, we can infer the direction of cell migration. We also observed the distribution of focal adhesions (FAs) by staining paxillin (Figure S3, Supporting Information). From the figure, we can see that, for cells on the anisotropic membrane, FAs distributed along the direction of underlying nanofibers. For cells on the random and planar membranes, distributions of FAs were more uniform. These results strongly indicated that anisotropic nanofibrous membranes could affect the cell morphology and cytoskeleton/FA distribution, which could, in turn, have an obvious impact on cell migration.

CONCLUSION

In conclusion, we fabricated bioinspired anisotropic nanofibrous membranes that facilitate cell attachment and directional migration for rapid wound healing. The natural scab contains anisotropic nanofibers that cover the wound area. This feature was exploited to fabricate wound dressing materials with anisotropic nanostructures by electrospinning. Anisotropic nanofibrous membranes showed a good affinity for cells and promoted directional cell migration for cells that are involved in wound repair, which is more advantageous compared to the random nanofibrous and planar membranes. Thus, this cytophilic anisotropic nanofibrous membrane is of great potential in the fabrication of dressing materials for rapid wound healing, as well as other biomaterials,[28−32] such as membranes for the capture of circulating tumor cells, bone growth, and construction of a neural network.

ASSOCIATED CONTENT

Supporting Information

SEM image of a Band-aid, viability of HUVECs after incubation with various substrates, and fluorescent images of the distribution of paxillin in HUVECs on membranes. This material is available free of charge via the Internet at http://pubs.acs.org.

AUTHOR INFORMATION

Corresponding Author

*E-mail: stwang@iccas.ac.cn.

Author Contributions

Y.X., H.D., and K.S. contributed equally to the work.

Notes

The authors declare no competing financial interest.

ACKNOWLEDGMENTS

This work was supported by the National Research Fund for Fundamental Key Projects (Grants 2012CB933800, 2011CB935700, and 2012CB933200), National Natural Science Foundation (Grants 21175140, 20974113, 21121001, 21222309, 21071148, and 21271182), Key Research Program of the Chinese Academy of Sciences (Grant KJZD-EW-M01), and China Postdoctoral Science Foundation (Grant 2012M510555).

REFERENCES

(1) Martin, P. *Science* **1997**, *276*, 75−81.
(2) Zahir, M. *Br. J. Surg.* **1965**, *52*, 376.

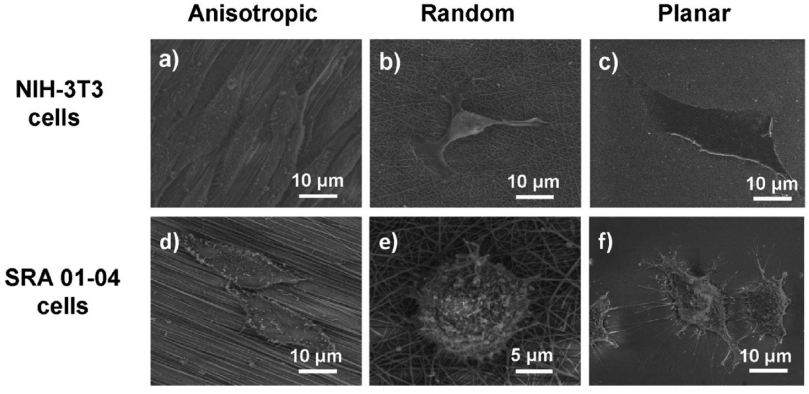

Figure 6. ESEM images of NIH 3T3 and SRA 01-04 cells on the anisotropic, random, and planar PU membranes after being cultured for 24 h. NIH 3T3 and SRA 01-04 cells exhibit flat and bipolar morphologies on the anisotropic nanofibrous membranes (a and d). For cells seeded on the random nanofibrous membranes, NIH 3T3 cells exhibit polygonal shape (b), while SRA01-04 cells became round (e). Both cells show polygonal shape on the planar membranes (c and f).

(3) Agren, M. S.; Taplin, C. J.; Woessner, J. F.; Eaglstein, W. H.; Mertz, P. M. *J. Invest. Dermatol.* **1992**, *99*, 709−714.
(4) Balasubramani, M.; Kumar, T. R.; Babu, M. *Burns* **2001**, *27*, 534−544.
(5) Cai, F. Y.; Shimooka, N.; Ohnishi, Y. I.; Yoshimine, T. *Surg. Neurol.* **2008**, *70*, 217−220.
(6) Murakami, K.; Aoki, H.; Nakamura, S.; Nakamura, S.; Takikawa, M.; Hanzawa, M.; Kishimoto, S.; Hattori, H.; Tanaka, Y.; Kiyosawa, T.; Sato, Y.; Ishihara, M. *Biomaterials* **2010**, *31*, 83−90.
(7) Qin, Y. M. *Polym. Int.* **2008**, *57*, 171−180. Mi, L.; Xue, H.; Li, Y. T.; Jiang, S. Y. *Adv. Funct. Mater.* **2011**, *21*, 4028−4034.
(8) Seetharaman, S.; Natesan, S.; Stowers, R. S.; Mullens, C.; Baer, D. G.; Suggs, L. J.; Christy, R. J. *Acta Biomater.* **2011**, *7*, 2787−2796.
(9) Vargas, E. A. T.; Baracho, N. C. D.; de Brito, J.; de Queiroz, A. A. A. *Acta Biomater.* **2010**, *6*, 1069−1078.
(10) Lindner, H. B.; Zhang, A. G.; Eldridge, J.; Demcheva, M.; Tsichilis, P.; Seth, A.; Vournakis, J.; Muise-Helmericks, R. C. *PLoS One* **2011**, *6*.
(11) El-Halfawy, O. M.; El-Gowelli, H. M.; Aloufy, A. K.; Boraei, N. A.; El-Khordagui, L. K. *Eur. J. Pharm. Biopharm.* **2012**, *80*, 85−94.
(12) Barrientos, S.; Stojadinovic, O.; Golinko, M. S.; Brem, H.; Tomic-Canic, M. *Wound Repair Regen.* **2008**, *16*, 585−601.
(13) Stevens, M. M.; George, J. H. *Science* **2005**, *310*, 1135−1138.
(14) Mertaniemi, H.; Laukkanen, A.; Teirfolk, J. E.; Ikkala, O.; Ras, R. H. A. *RSC Adv.* **2012**, *2*, 2882−2886.
(15) Li, D.; Xia, Y. N. *Adv. Mater.* **2004**, *16*, 1151−1170.
(16) Santerre, J. P.; Woodhouse, K.; Laroche, G.; Labow, R. S. *Biomaterials* **2005**, *26*, 7457−7470.
(17) Zhao, F.; Zhao, Y.; Liu, Y.; Chang, X. L.; Chen, C. Y.; Zhao, Y. L. *Small* **2011**, *7*, 1322−1337.
(18) Qu, J.; Zhou, D. D.; Xu, X. J.; Zhang, F.; He, L. H.; Ye, R.; Zhu, Z. Y.; Zuo, B. Q.; Zhang, H. X. *Appl. Surf. Sci.* **2012**, *261*, 320−326.
(19) Beachley, V.; Katsanevakis, E.; Zhang, N.; Wen, X. J. *Adv. Polym. Sci.* **2012**, *246*, 171−212.
(20) Diegelmann, R. F.; Evans, M. C. *Front. Biosci.* **2004**, *9*, 283−289.
(21) Goetsch, K. P.; Niesler, C. U. *Anal. Biochem.* **2011**, *411*, 158−160.
(22) Xie, Y. Y.; Zhang, W.; Wang, L. M.; Sun, K.; Sun, Y.; Jiang, X. Y. *Lab Chip* **2011**, *11*, 2819−2822.
(23) Kim, H. N.; Hong, Y.; Kim, M. S.; Kim, S. M.; Suh, K. Y. *Biomaterials* **2012**, *33*, 8782−8792.
(24) Eiseler, T.; Doppler, H.; Yan, I. K.; Kitatani, K.; Mizuno, K.; Storz, P. *Nat. Cell Biol.* **2009**, *11*, 545−U64.
(25) Turner, C. E. *Nat. Cell Biol.* **2000**, *2*, E231−E236.
(26) Ballestrem, C.; Wehrle-Haller, B.; Imhof, B. A. *J. Cell Sci.* **1998**, *111*, 1649−1658.
(27) Welch, M. D.; Mallavarapu, A.; Rosenblatt, J.; Mitchison, T. J. *Curr. Opin. Cell Biol.* **1997**, *9*, 54−61.
(28) Liu, X. H.; Jin, X. B.; Ma, P. X. *Nat. Mater.* **2011**, *10*, 398−406.
(29) Gunn, J.; Zhang, M. Q. *Trends Biotechnol.* **2010**, *28*, 189−197.
(30) Wang, S. T.; Wang, H.; Jiao, J.; Chen, K. J.; Owens, G. E.; Kamei, K. I.; Sun, J.; Sherman, D. J.; Behrenbruch, C. P.; Wu, H.; Tseng, H. R. *Angew. Chem., Int. Ed.* **2009**, *48*, 8970−8973.
(31) Chen, L.; Liu, X. L.; Su, B.; Li, J.; Jiang, L.; Han, D.; Wang, S. T. *Adv. Mater.* **2011**, *23*, 4376−4380.
(32) Mukhatyar, V. J.; Salmeron-Sanchez, M.; Rudra, S.; Mukhopadaya, S.; Barker, T. H.; Garcia, A. J.; Bellamkonda, R. V. *Biomaterials* **2011**, *32*, 3958−3968.